JOURNAL OF SOLID STATE CHEMISTRY **139,** 290–298 (1998)
ARTICLE NO. SC987843

Novel Synthesis Process and Structural Characterization of Li–Mn–O Spinels

Toshimi Takada,[1] Hirotoshi Enoki, Hiroshi Hayakawa, and Etsuo Akiba

National Institute of Materials and Chemical Research, Higashi 1-1, Tsukuba, Ibaraki 305, Japan

Received August 25, 1997; revised form December 30, 1997; accepted March 31, 1998

A new process for the synthesis of well-crystallized lithium manganese spinels with a homogenous composition $Li_{1+x}Mn_{2-x}O_4$ ($0 \le x \le 0.333$) has been developed using the stoichiometry mixture of lithium acetate LiOAc and manganese nitrate $Mn(NO_3)_2$ as starting materials. The decomposition of the raw materials and the stoichiometry mixture was studied using TG–DTA; the formation of lithium manganospinels occurs below 400°C. The crystallites appear to be single crystals in SEM micrographs. The size of the crystallites was in the range of 0.1 to 2.0 μm and depended on the synthesis conditions. The crystal structure of these compounds was studied using X-ray powder diffraction and Rietveld refinement. The lattice parameter and manganese occupancy at 16*d* sites in the space group $Fd\bar{3}m$ are sensitive to both the synthesis temperature and the composition of the spinels (Li/Mn ratio) as a result of the variation in manganese valency. Synthesis temperature, atmosphere, and the Li/Mn ratio in the starting materials are the key issues for control of the manganese valency in spinel $Li_{1+x}Mn_{2-x}O_4$ ($0 \le x \le 0.333$) for use in rechargeable lithium batteries. © 1998 Academic Press

Key Words: **Spinel; structure refinement; lithium manganese oxides; Rietveld method; lithium batteries.**

1. INTRODUCTION

The commercial lithium ion batteries which use $LiCoO_2$ as cathode and graphite or carbon as anode have come into wide use as the power for portable/commercial electronics. Their high energy density (120 Wh/g) and good cycle life (500–1000 cycles) make them very attractive for use in energy storage and in powering emission-free vehicles in the near future. In order to overcome the resource limitation and thus the high cost of Co, lithium manganese oxide spinels are being extensively studied as a promising candidate for the replacement of $LiCoO_2$.

Recent research (1–5) has clarified that the stoichiometric spinels $Li[Li_xMn_{2-x}]O_4$ ($0.0 \le x \le 0.333$) with end members $LiMn_2O_4$ and $Li_4Mn_5O_{12}$, are of particular significance among Li–Mn–O compounds because they can be used as insertion electrodes for rechargeable 3 and 4 V lithium batteries. The spinels with low x ($0.0 \le x \le 0.10$) are of interest for 4 V lithium cells, whereas those with a high value of x are of interest for 3 V lithium cells. Extraction of Li from the tetrahedral sites (8*a* sites) in $Li_{1-y}[Li_xMn_{2-x}]O_4$ occurs at 4 V over the range $0.0 \le y \le (1 - 3x)$, until the manganese oxidation state reaches 4.0. The cubic symmetry of the $Li_{1-y}[Li_xMn_{2-x}]O_4$ structure is maintained throughout this reaction. Spinels with a higher value of x ($x > 0.05$) show better cyclability than those with lower x, whereas the excess lithium reduces the capacity because the amount of Li which can be removed during the charging process is less than $(1.0 - 3x)$ per formula unit. Therefore, controlling the value of x is crucial in producing high quality $Li[Li_xMn_{2-x}]O_4$ in term of capacity and cycle life for 4 V lithium cells. On the other hand, Li insertion into $Li_{1+y}[Li_xMn_{2-x}]O_4$ occurs at 3 V for the range $0.0 \le y \le 1$, in this reaction the value of y is independent of x. $Li_4Mn_5O_{12}$ is being considered as an ideal compound for 3 V cells because spinels with Mn oxidation state close to 4+ showed better capacity retention during cycling than $LiMn_2O_4$, in which the average Mn oxidation state is 3.5+.

It is the current consensus that a wide range of solid solution exists within the Li–Mn–O family of spinel compounds, and that the composition of the spinel electrode plays a very important role in controlling the rechargeability of the electrode (4). Therefore, attention should be paid to the control of the synthesis process to obtain single phase samples with the required stoichiometry. Understanding the structural changes during the synthesis process is crucial for both process control and comprehension of the variation of voltage, capacity, and cycling performance of Li/spinel cells.

Research (1–3) indicates that the spinel lattice parameter varies with both the composition and the synthesis conditions of the solid state reactions, but such information was limited to samples $Li_{1+x}Mn_{2-x}O_4$ prepared under certain conditions. The composition uncertainty inside each crystallite remains to be considered. On the other hand, many

[1] To whom correspondence should be addressed. E-mail: takada@nimc.go.jp.

0022-4596/98 $25.00

reports (6–10) dealt with the low temperature synthesis processes using the solution techniques, which possess the advantage of homogeneity of the spinel composition and control of the grain size over the solid state reactions. The main problem with such low temperature processes is how to ensure the crystallinity of the particles, in order to obtain decent electrode performance. Systematic crystallographic studies of samples synthesized under various conditions are indispensable in understanding the differences in the electrode performance of Li–Mn–O spinels as reported in recent articles (9 and 10).

In this study, we have developed a new synthesis process to obtain well-crystallized lithium manganospinels with a homogenous composition $Li_{1+x}Mn_{2-x}O_4$ ($0 \le x \le 0.333$). The crystallites in the final products were observed using FE–SEM. Attention was paid to the effect of synthesis temperature and to the Li/Mn ratio in the starting materials on the spinel structure of the crystallites. Redox titration, powder X-ray diffraction, and Rietveld refinement were conducted to clarify the relations between the spinel lattice parameter, the Mn occupancy at 16*d* sites, and the average oxidation state of manganese. The optimization of the synthesis conditions of spinel $Li_{1+x}Mn_{2-x}O_4$ for rechargeable lithium batteries is discussed.

2. EXPERIMENTAL

2.1. Synthesis of Well-Crystallized Li–Mn–O Spinels

Ninety-nine percent pure lithium acetate $LiOAc \cdot 2H_2O$, and manganese nitrate $Mn(NO_3)_2 \cdot 6H_2O$ (from WAKO Pure Chemical Industries, Ltd.) were used as starting materials. The raw materials with a molar ratio Li/Mn of 1/2, 3/5, 5/7, and 4/5, were first heated at 100°C to obtain a uniform solution and then slowly oxidized at 200–250°C under flowing O_2 to convert the stoichiometric solution to a solid Li–Mn–O precursor. The precursor was then ground and pelletized ($\varnothing 10 \times 10$ mm) before heating at a temperature ranging from 400 to 900°C for 1 to 3 days. All samples were heated at a rate of 100°C/h and slowly cooled to room temperature in the furnace (about 7 h) under flowing O_2 (200 ml/min). Details of the preparation process were described in our previous reports (11, 12).

2.2. Thermal Analysis

Thermogravimetry and differential thermal analysis (TG–DTA) were performed on the raw materials and their eutectic mixtures using a Rigaku thermal plus TG8120. Samples of 10–30 mg were placed in Al_2O_3 crucibles and heated at a heating/cooling rate of 5 or 10°C/min under 100 ml/min flow of oxygen. 99.9% pure Al_2O_3 powder was used as a standard.

2.3. X-Ray Diffraction

X-ray powder diffraction measurements were conducted at room temperature on a Rigaku RAX-I X-ray diffractometer with monochromatized Cu$K\alpha$ radiation ($\lambda =$ 1.5406 Å) at 40 kV, 30 mA. The scan data were collected at a rate of 0.5°/min in the 2θ range of 10° to 90°. Data for the Rietveld refinements were collected between $2\theta = 15°–120°$ with a step interval of 0.02°. Structural refinements were carried out with a Rietveld refinement program RIETAN-97 β version (13, 14).

2.4. Electron Microscopy

Scanning electron micrographs were taken at room temperature on a Hitachi S-800 microscope equipped with a field emission gun, at 10 kV. The specimen was coated with about 5 to 10-nm thick Pt for observation. The size distribution profiles were obtained by counting more than 200 particles in the SEM pictures for each sample with a 10× magnifying glass.

2.5. Redox Titration

The average oxidation state of Mn (Mn valency hereafter) in the final spinel products was determined from the active oxygen content as measured by the standard volumetric method (15). The standard aqueous solution of $H_2C_2O_4$ was prepared by dissolving 10 g of the standard 99.99% pure $Na_2C_2O_4$ in a 500-ml volumetric flask filled with pure water and 100 ml concentrate H_2SO_4 (1 : 1 in volume). Li–Mn–O spinel samples (about 0.1 g) were dissolved into an excess of 10 ml $Na_2C_2O_4$ (2 w/v%) and 10 ml H_2SO_4 (1 : 4 in volume) around 65°C in a water bath to reduce all the Mn^{n+} to Mn^{2+}. The excess $C_2O_4^{2-}$ in the solution was determined by titration at 65°C with a standard solution of $KMnO_4$ (0.02 mol/l from WAKO Pure Chemical Industries, Ltd.).

3. RESULTS AND DISCUSSION

3.1. Decomposition of the Raw Materials and Spinel Formation

Figure 1 shows the TG–DTA curves of $LiOAc \cdot 2H_2O$, $Mn(NO_3)_2 \cdot 6H_2O$ and their eutectic mixture with a Li/Mn ratio of 3/5 (designated as Spinel 3/5). TG curves indicate that weight loss occurs mainly in two steps at temperatures ranging from room temperature to 180°C, and thereafter corresponding to the dehydration and decomposition, respectively. For $LiOAc \cdot 2H_2O$, two extra sharp endothermic peaks, around 50 and 275°C, are clearly observed in the DTA trace, in good agreement with the melting point of $LiOAc \cdot 2H_2O$ and the dehydrated LiOAc, respectively. Hence, the endothermic peak from 100 to 170°C can be attributed to the dehydration. The weight loss of 36.2%

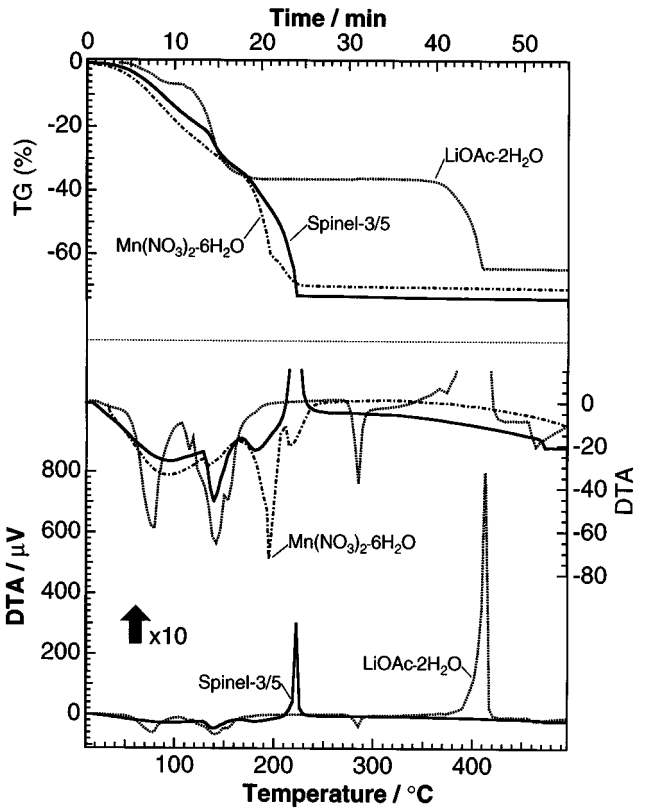

FIG. 1. TG–DTA curves for the raw materials of $LiOAc \cdot 2H_2O$ and $Mn(NO_3)_2 \cdot 6H_2O$, and their stoichiometric mixture with a $Li/Mn = 3/5$ (Spinel 3/5).

in the first step is consistent with the dehydration of $LiOAc \cdot 2H_2O$ to LiOAc (35.3%) within the experimental error. The strong exothermic peak at 400°C corresponds to the decomposition of the dehydrated LiOAc to Li_2CO_3, which leads to a weight loss of 28.05%. The dehydration of $Mn(NO_3)_2 \cdot 6H_2O$ proceeds rather slowly up to 180°C and the decomposition starts as soon as the dehydration is complete. In contrast to LiOAc, the decomposition of $Mn(NO_3)_2$ is endothermic. The detected total weight loss was 70.3%, which corresponds to the decomposition of $Mn(NO_3)_2 \cdot 6H_2O$ to MnO_2 (69.7%). For the eutectic mixture Spinel-3/5, the dehydration proceeded according to the individual compounds. However, the decomposition occurred at 220°C which is a little higher than that of $Mn(NO_3)_2$ but much lower than that of LiOAc. A weak endothermic peak appears at the very start of the reaction, then a strong exothermic peak follows. The total weight loss of 72.88% agrees well with the formation of lithium mangano-oxides (72.5% to $Li_2O + MnO_2$) rather than $Li_2CO_3 + MnO_2$ (68.8%). In fact, Li_2CO_3 was not detected in this Li–Mn–O precursor by X-ray diffraction. A clear spinel diffraction pattern was detected for the sample heat-treated at 300°C.

In summary, the decomposition of $LiOAc \cdot 2H_2O$, $Mn(NO_3)_2 \cdot 6H_2O$ and their eutectic mixture under flowing oxygen is described

$$2LiOAc \cdot 2H_2O \xrightarrow{<170^\circ C} 2LiOAc + 4H_2O\uparrow \quad \xrightarrow[\geq 400^\circ C]{} Li_2CO_3 + 3CO_2\uparrow + 3H_2O\uparrow \qquad [1]$$

$$Mn(NO_3)_2 \cdot 6H_2O \xrightarrow{<180^\circ C} Mn(NO_3)_2 + 6H_2O\uparrow \quad \xrightarrow[\geq 180^\circ C]{} MnO_2 + 2NO_2\uparrow \qquad [2]$$

$$\text{Eutectic Mixture} \xrightarrow{\geq 220^\circ C} Li_2O + MnO_2 \xrightarrow{\geq 300^\circ C} Li_{1+x}Mn_{2-x}O_4. \qquad [3]$$

To confirm Eq. [3] and compare the new process with the conventional solid state reaction process, TG–DTA curves for the mixture of different raw materials ($Li/Mn = 4/5$) are shown in Fig. 2. From the curves for $Li_2CO_3 + MnO_2$, clearly, the full decomposition of Li_2CO_3 occurs around 710°C because the first endothermic peak around 570°C corresponds to the transition $MnO_2 \rightarrow Mn_2O_3$. For $Li_2CO_3 + MnCO_3$, the decomposition of $MnCO_3 \rightarrow MnO_2$ starts at 330°C, while Li_2CO_3 remains up to 760°C.

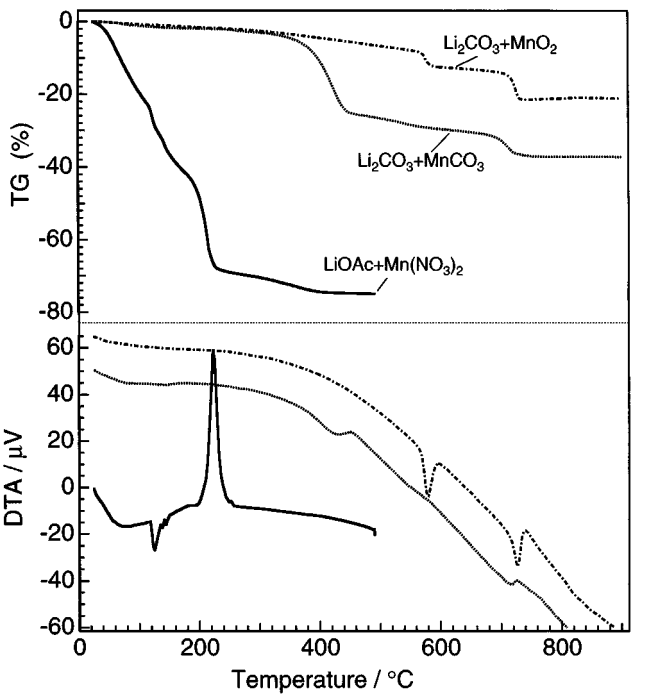

FIG. 2. TG–DTA curves for the mixture of raw materials with a $Li/Mn = 4/5$: $Li_2CO_3 + MnO_2$, $Li_2CO_3 + MnCO_3$, and $LiOAc + Mn(NO_3)_2$, respectively.

Therefore, once Li_2CO_3 forms, it will remain up to a temperature higher than 700°C, hence it is difficult to obtain pure spinel phase at a temperature below 700°C when using Li_2CO_3 as the raw material. For the eutectic LiOAc + $Mn(NO_3)_2$, the decomposition reactions complete at a temperature as low as 350°C. Consequently, the formation of Li_2CO_3 does not occur during the decomposition of the eutectic mixture, and the spinel $Li_4Mn_5O_{12}$ can be easily synthesized using our new process (11, 16). It is not clear why lithium acetate decomposition in the presence of manganese nitrate does not result in carbonate product. The formation of a Li–Mn complex before the decomposition/oxidation occurs is considered to be responsible for this, and thus, the decomposition temperature drops to 220°C from 400°C.

3.2. Synthesis of Well-Crystallized Li–Mn–O Spinels

Figure 3 shows the powder X-ray diffraction patterns of Li–Mn–O spinels prepared at 400, 500, 650, 800, and 900°C from the stoichiometric mixture of LiOAc and $Mn(NO_3)_2$, with a Li/Mn ratio of 1/2, 3/5, 5/7, or 4/5. We confirmed that the composition of the final products agrees well with the nominal Li/Mn ratio in the precursor by the atomic absorption analyses (11). The loss of lithium was not detected by TG–DTA up to a temperature of 930°C under flowing oxygen (12). Clearly, these samples all possess a spinel structure, the higher synthesis temperature gave sharper and higher diffraction peaks, and consequently a better crystallinity for the spinel Li–Mn–O phase. To clearly show the difference between these samples, the enlarged XRD profiles are given in Fig. 4. For 400°C samples, a pure spinel phase forms in the sample with a Li/Mn = 4/5, with diffraction peaks at $2\theta = 36.6°, 44.6°$, corresponding to the lattice planes (311) and (400) of the spinel $Li_4Mn_5O_{12}$. The intensity of these peaks diminishes with the decrease in the Li/Mn ratio. On the contrary, the diffraction peaks of the minority phase Mn_2O_3 increased. Therefore, at temperatures below 400°C under flowing oxygen, the formation of a spinel structure similar to $Li_4Mn_5O_{12}$ occurs independently of the starting Li/Mn ratio. At temperatures between

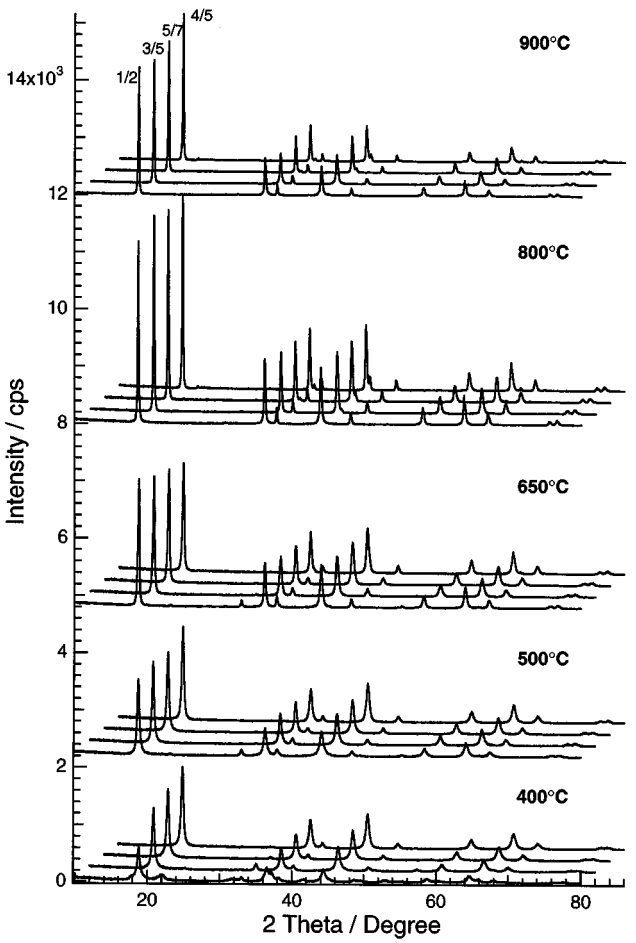

FIG. 3. X-ray diffraction patterns for the Li–Mn–O spinels prepared at temperatures ranging from 400 to 900°C under flowing oxygen using $LiOAc \cdot 2H_2O$ and $Mn(NO_3)_2 \cdot 6H_2O$ as starting materials. For clarity, intensity offset applied.

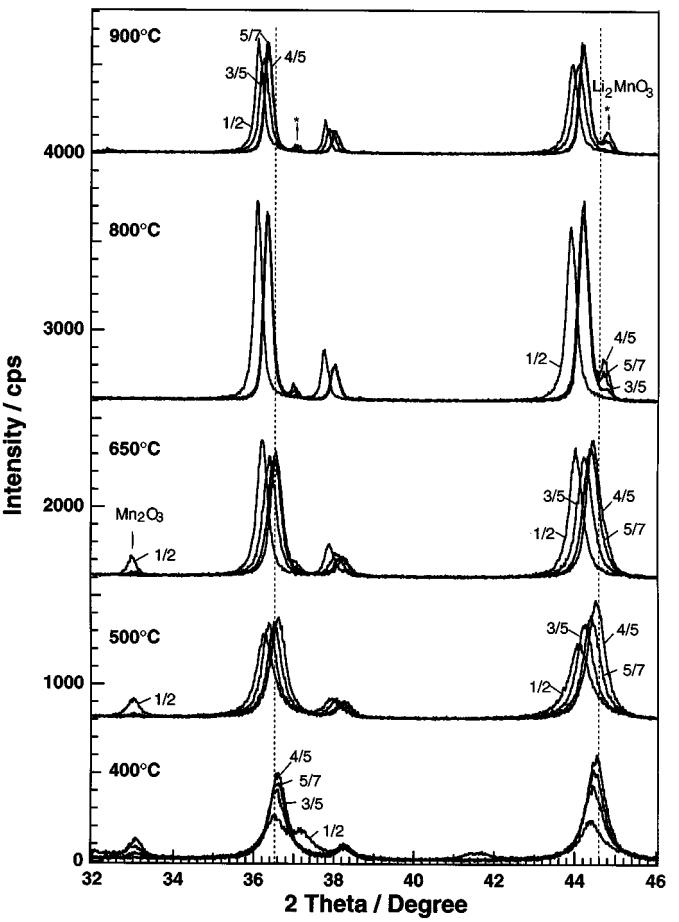

FIG. 4. Partially enlarged X-ray diffraction patterns given in Fig. 3. Arrows indicate the reflections from the minority phases Mn_2O_3 or Li_2MnO_3.

500 and 650°C, the diffraction peaks at $2\theta = 36.6°$, 44.6°, shift to lower angles with the decrease of Li/Mn in the precursor, which indicates the formation of pure spinel phases with a composition $Li_{1+x}Mn_{2-x}O_4$ ($0 < x \leq 0.333$) in accordance with the composition of the precursor. A minority phase Mn_2O_3, however was detected in samples with Li/Mn = 1/2, indicating that pure $LiMn_2O_4$ is difficult to prepare at temperatures below 650°C under flowing oxygen. At higher temperatures (800–900°C), the diffraction peaks from Mn_2O_3 disappear in all samples, hence pure spinels form for samples with Li/Mn $\leq$ 3/5. For the samples with Li/Mn > 3/5, however, a minority monoclinic phase Li_2MnO_3 appears, accompanied by a shift of the diffraction peaks of the spinel to lower angles.

Figure 5 shows a typical SEM image of the spinel $Li_{1+x}Mn_{2-x}O_4$ crystallites in the samples prepared at various temperatures. At temperatures below 650°C, the crystallites are rather small, only spherical particles with a size between 0.04 and 0.3 μm are observed. At higher temperatures, well-developed polyhedra (mainly octahedra bounded by eight (111) planes, are clearly observed. The particles appear just as those of single-crystal-like gold which also have a cubic lattice. The size of the crystallites increase from 0.2 to 2 μm as the synthesis temperature is increased from 800 to 900°C. Typical size distributions for the crystallites in these samples are given in Fig. 6a. Obviously, the smaller the crystallites, the sharper the size distribution profiles are. Figure 6b shows that the average size of the crystallites increases as a function of the synthesis temperature. At temperatures below 800°C, the growth of the crystallites is rather slow, but it becomes much faster at elevated temperatures as a result of the rapid diffusion of Li or Mn atoms. Figure 7 shows the SEM micrographs for the samples synthesized at 900°C. The appearance of the

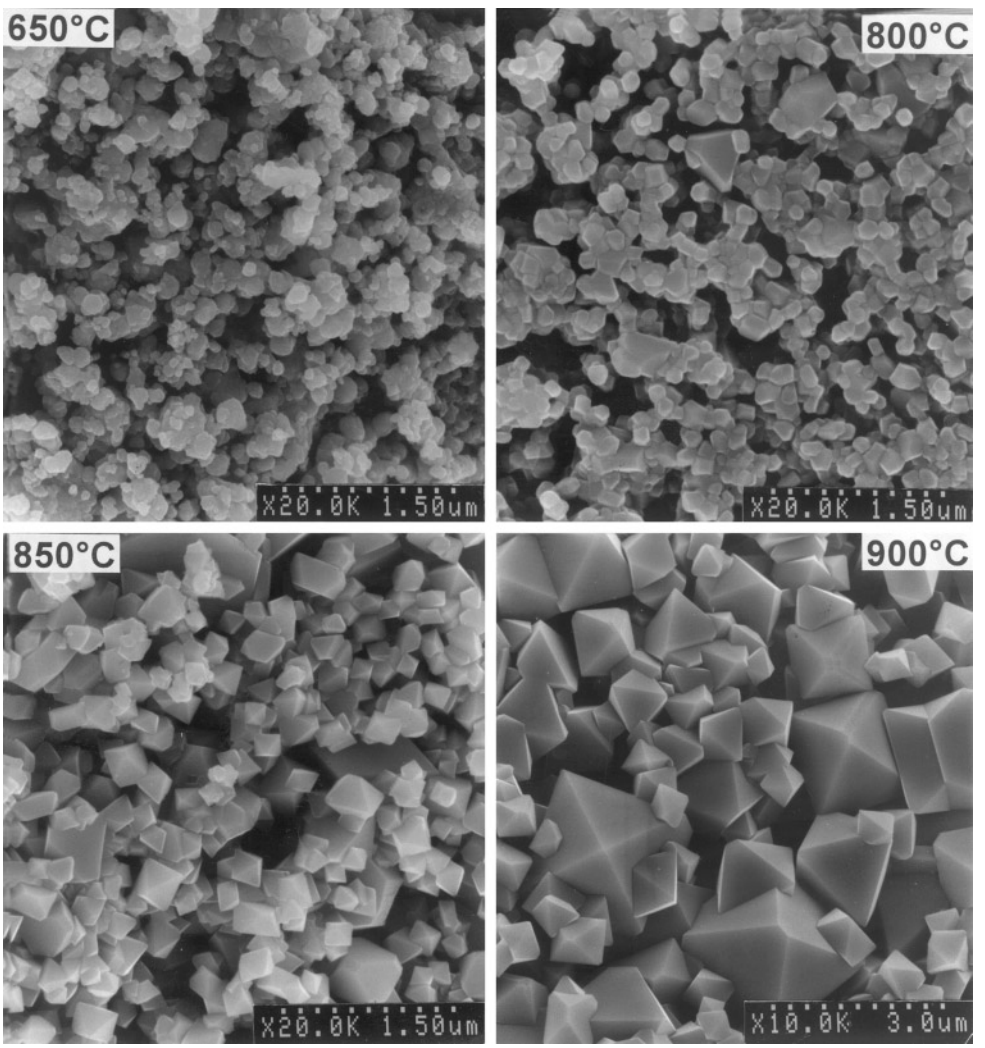

FIG. 5. Typical SEM micrographs of the Li–Mn–O spinel crystallites in the samples prepared at a temperature between 650 and 900°C.

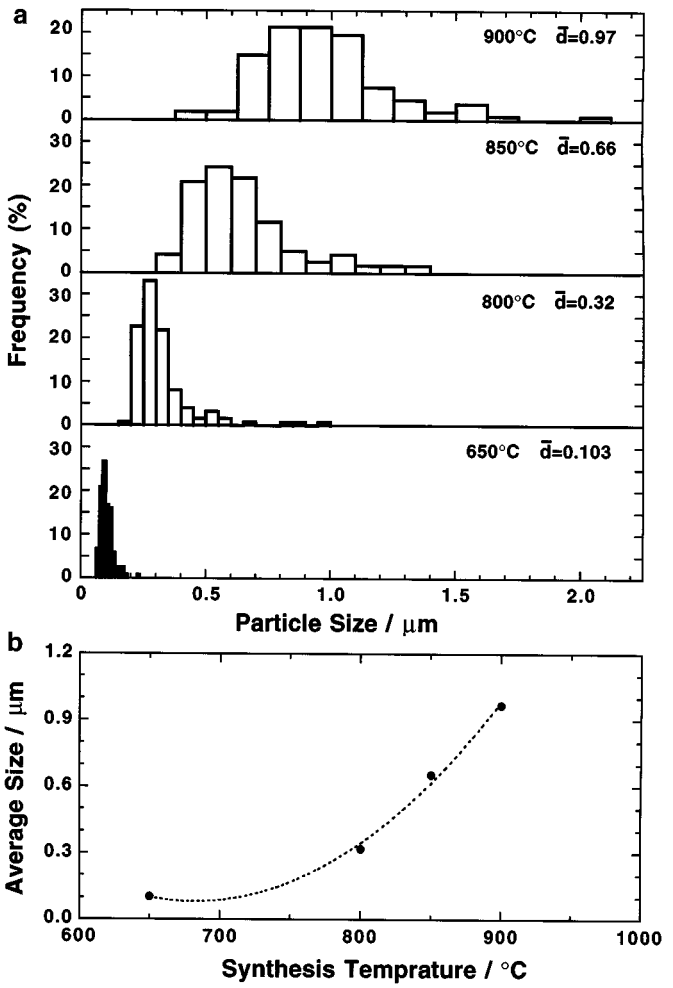

FIG. 6. (a) Representative size distributions of the Li–Mn–O crystallites in the samples synthesized at temperatures ranging from 650 to 900°C, and (b) the growth of the particle size as a function of the synthesis temperature.

crystallites in these samples is basically the same, they are all in single-crystal-like forms. It appears that crystallites grew faster as the Li/Mn increased from 1/2 to 4/5 in the precursor. Further study on the crystal growth is in progress.

3.3. Structural Changes of Li–Mn–O Spinels

Rietveld refinements were carried out for all samples synthesized at temperatures between 400 and 900°C, using the space group $Fd\bar{3}m$. For 800–900°C samples with a Li/Mn = 5/7 or 4/5, the refinements included two crystalline phases: spinel $Li[Li_xMn_{2-x}]O_4$ and Li_2MnO_3 ($C/2m$). Details of the procedure are described in our previous reports (11, 16). We have focused on the lattice parameter, manganese occupancy at the 16*d* sites, and oxygen parameter (atomic coordinates). Isotropic thermal parameters of Li and O were initially fixed at values determined using the neutron diffraction data for $Li_4Mn_5O_{12}$ and refined in the final refinements. The occupancy of Li at the 8*a* sites was fixed at 1.0. Allowing variation of the oxygen site occupancy results in a value of 1.0 within the estimated standard deviation (e.s.d.), which indicates that the spinel phase in these samples is very nearly stoichiometric with respect to oxygen.

The refined lattice parameter and the occupancy of manganese at the 16*d* site, g(Mn), are plotted against the Li/Mn ratio in the precursors in Figs. 8a and 8b, respectively. Regardless of the synthesis temperatures, the spinel lattice parameter decreases in proportion to the Li/Mn ratio. Accordingly, the refined g(Mn) decreases with the Li/Mn ratio. The line designated as ideal for g(Mn) was calculated from the ratio of Li/Mn corresponding to the stoichiometric spinel $(Li)_{8a}[Li_xMn_{2-x}]_{16d}O_4$ $(0.0 \le x \le 0.333)$. Clearly, for Li/Mn ≤ 0.6, g(Mn) is very close to that of single phase $(Li)_{8a}[Li_xMn_{2-x}]_{16d}O_4$ with $0.0 \le x \le 0.125$, except those samples synthesized at a temperature below 650°C. In contrast, when Li/Mn > 0.6, g(Mn) is very close to that of single phase $(Li)_{8a}[Li_xMn_{2-x}]_{16d}O_4$ with $0.125 < x \le 0.333$ at temperatures below 650°C, but deviated from the line ideal as synthesis temperature was raised above 800°C. To confirm this result, the average oxidation state of manganese in these samples was determined by redox titration. Results are given in Fig. 8c, along with the line ideal calculated for the stoichiometric $(Li)_{8a}[Li_xMn_{2-x}]_{16d}O_4$ $(0 \le x \le 0.333)$. Strict correspondence of Mn valency with g(Mn) was obtained, verifying the validity of the refined g(Mn) from XRD data using Rietveld method, and the formation of spinel phase with a composition close to $Li[Li_xMn_{2-x}]_{16d}O_4$ $(0 \le x < 0.333)$. Note the Mn valency was found to be somehow lower than 4.0 in those samples with Li/Mn = 4/5, which indicates the difficulty to synthesize perfect $Li_4Mn_5O_{12}$ with 100% Mn in the 4+ state. To clearly show the changes of the lattice parameter, g(Mn), and the Mn valency, we did not plot the errors of these data in Fig. 8 but in Fig. 9.

To better understand the effect of synthesis temperature on the spinel structure, we replotted the spinel lattice parameter and the refined g(Mn) in Fig. 9 as a function of synthesis temperature, along with the Mn valency. Clearly, synthesis temperature strongly affects the spinel structure in all samples with Li/Mn ranging from 1/2 to 4/5. As a result, higher synthesis temperature gives a larger lattice parameter. The g(Mn) at 16*d* sites increased with increasing temperature, whereas the Mn valency decreased accordingly. The increase of the lattice parameter with the synthesis temperature can therefore be ascribed to the reduction of a part of Mn^{4+} to Mn^{3+} at elevated temperatures because Mn^{3+} ions are more stable than Mn^{4+} at temperatures above 580°C, and the effective ionic radii of octahedrally coordinated Mn^{3+} ions (0.645, at high spin state) is larger than that of Mn^{4+} (0.56 Å). Recent study on

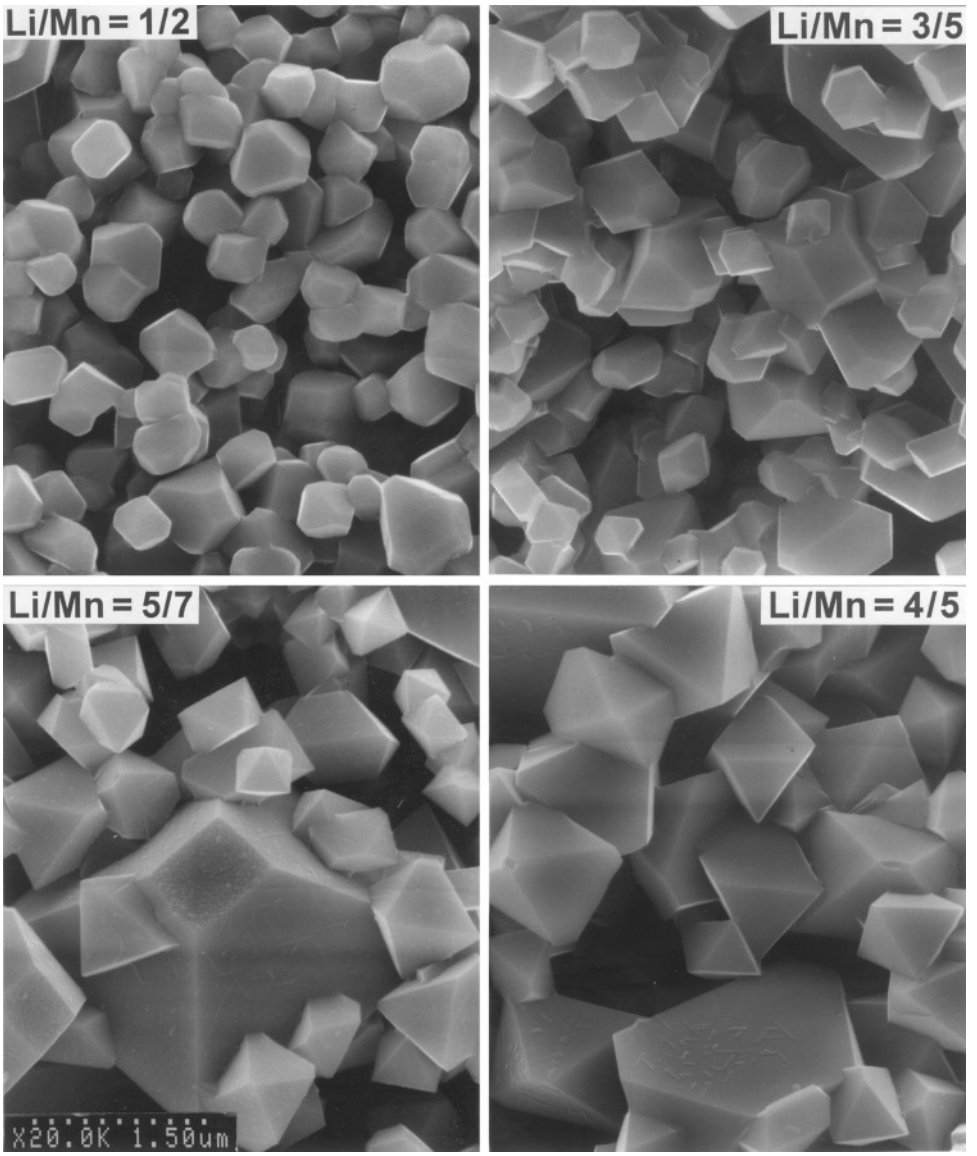

FIG. 7. SEM micrographs of Li–Mn–O spinel crystallites in the samples synthesized at 900°C with a Li/Mn of 1/2, 3/5, 5/7, and 4/5 in the precursor.

the magnetic properties of lithium manganospinels by Masquelier and co-workers (17) confirms that lower Mn oxidation states in a samples with the same Li/Mn results in a larger lattice parameter.

Figure 10 gives the oxygen parameter (the fractional coordinate of oxygen) of the spinel phase in these samples as a function of synthesis temperature. For all samples with Li/Mn ranging from 1/2 to 4/5, the oxygen parameter remains fairly constant at temperatures below 650°C, but it increases from 0.3870 to 0.3910 for higher temperatures, corresponding to the increase of the lattice parameter. These numbers are quite larger than the ideal value for the spinel structure, 0.375, which implies that Li–O tetrahedra are larger than the Mn–O octahedra (for simplicity, the Mn–O bond represents the bond between oxygen and the cations at the octahedral 16*d* sites). Larger values at elevated temperatures indicate that the Li–O bond is likely to be more ionic than the Mn–O bond and thus expands more readily with temperature.

Combining the results shown in Fig. 4 with those from the Rietveld refinements for spinel phase, we conclude that the formation of single phase spinel $(Li)_{8a}[Li_xMn_{2-x}]_{16d}O_4$ with $0 \leq x \leq 0.125$ occurs preferentially at temperatures 650–900°C, but it is difficult to obtain the single phase for those spinels with $0.125 < x \leq 0.333$ at temperatures higher than 800°C. At elevated temperatures, x in $(Li)_{8a}[Li_xMn_{2-x}]_{16d}O_4$ shifts to lower values and the precipitation of Li_2MnO_3, thus, occurs to consume the excess Li.

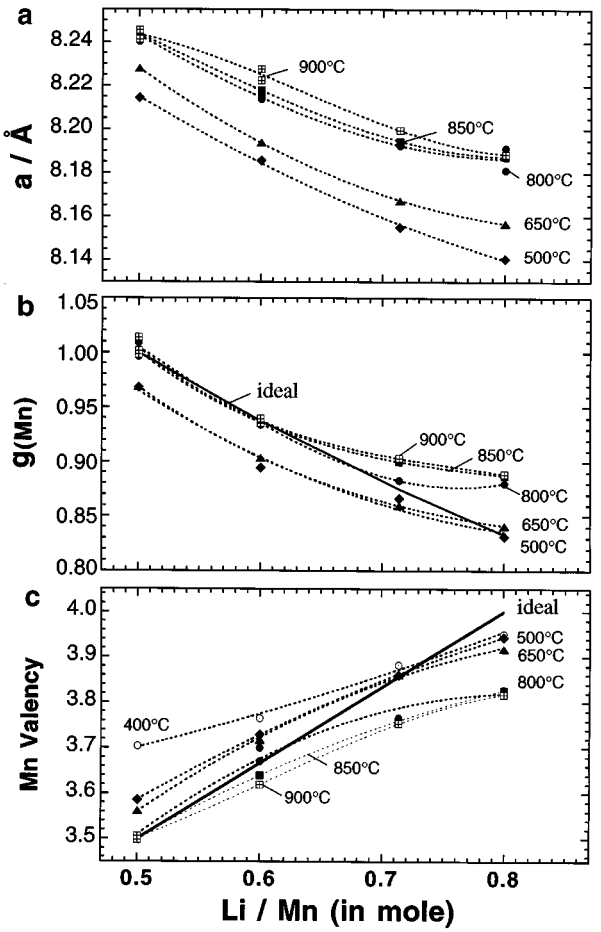

FIG. 8. Plot of the lattice parameter and the refined g(Mn) against the Li/Mn ratio in the precursors, along with the Mn valency determined by redox titration. For clarity, errors of these data were not plotted (see Fig. 9).

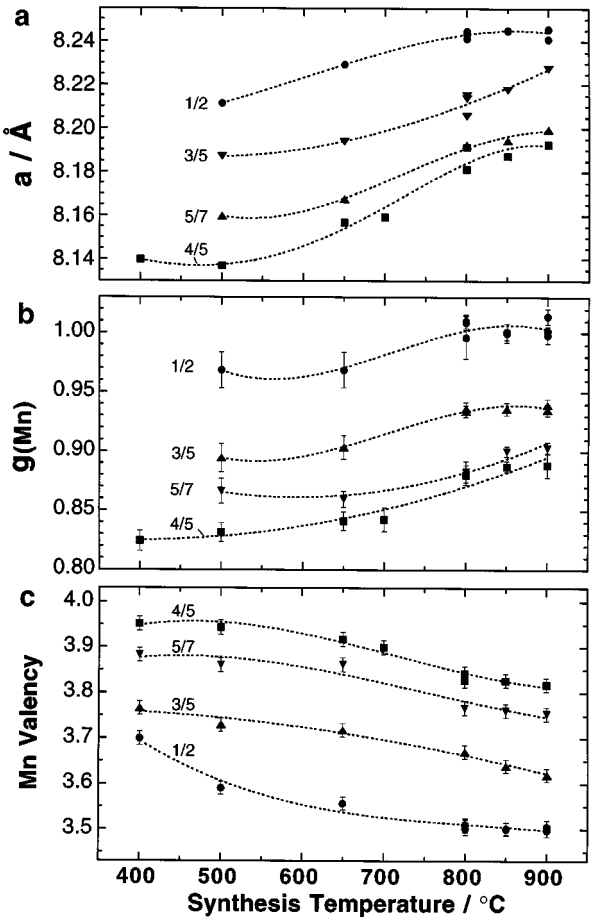

FIG. 9. Plot of the lattice parameter, refined g(Mn), and the Mn valency as a function of the synthesis temperature for samples with Li/Mn ranging from 1/2 to 4/5 in the precursors. Note errors of the lattice parameter are within the size of the marks at each point.

Therefore, the synthesis of such spinels with a single phase and good crystallinity is considered to be difficult. Based on the data for the Mn valency in Fig. 9c, we found that the atmosphere, i.e., the oxygen pressure, is also an important factor in the formation of pure spinel $Li_{1+x}Mn_{2-x}O_4$. Some preliminary data in this respect were given in a recent article of Yamada (18).

4. CONCLUSION

A new process for the synthesis of well-crystallized Li–Mn–O spinels $Li_{1+x}Mn_{2-x}O_4$ has been developed using the stoichiometric mixture of $LiOAc \cdot 2H_2O$ and $Mn(NO_3)_2 \cdot 6H_2O$ as starting materials. TG–DTA studies indicate that $LiOAc \cdot 2H_2O$ decomposes to Li_2CO_3 around 400°C, and $Mn(NO_3)_2 \cdot 6H_2O$ to MnO_2 under flowing oxygen at temperatures above 180°C. The decomposition of the stoichiometric mixture to Li–Mn–O compounds, however, occurs around 220°C under flowing oxygen. Heat treatments of the Li–Mn–O precursor at temperatures ranging from 400 to 900°C result in the formation of the spinel $Li_{1+x}Mn_{2-x}O_4$ ($0 \le x \le 0.333$). Single-crystal-like crystallites with size of 0.1–2.0 μm were observed in the samples synthesized at temperatures above 800°C. Using powder X-ray diffraction and Rietveld refinements, we were able to determine the spinel lattice parameter and the Mn occupancy at 16*d* sites, g(Mn). It was found that the lattice parameter and g(Mn) are dependent on both the synthesis temperature and the Li/Mn ratio in the precursor. Mn valency in the samples prepared at 400–900°C with a Li/Mn = 1/2–4/5 verified the reduction of a part of Mn^{4+} to Mn^{3+} at elevated temperatures independently of the Li/Mn ratio in the precursors. Formation of $Li_{1+x}Mn_{2-x}O_4$ with $0 \le x \le 0.125$ occurs at temperatures ranging from 650 to 900°C, but below 800°C for those with $0.125 < x < 0.333$. The synthesis temperature for pure $Li_4Mn_5O_{12}$ should

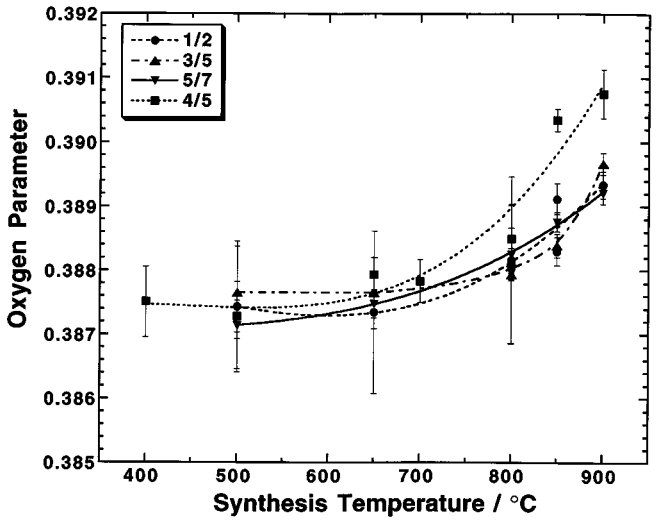

FIG. 10. Oxygen parameter for the samples synthesized at a temperature between 650 and 900°C with a Li/Mn ranging from 1/2 to 4/5 in the precursor.

be under 650°C. Particular attention should be given not only to the composition (Li/Mn of the precursor) but also to the synthesis conditions, such as, temperature and the atmosphere to control Mn valency and, therefore the structure of Li–Mn–O spinels for rechargeable lithium batteries.

ACKNOWLEDGMENTS

The authors thank Dr. Tatsuro Tsunoda for his helpful suggestion on FE–SEM microscopy and Dr. Pascal Tessier for reading and correcting this manuscript.

REFERENCES

1. J. M. Tarascon, W. R. McKinnon, F. Coowar, T. N. Bowmer, G. Amatucci, and D. Guyomard, *J. Electrochem. Soc.* **141,** 1421 (1994).
2. R. J. Gummow, A. de Kock, and M. M. Thackeray, *Solid State Ionics* **69,** 59 (1994).
3. Y. Gao and J. R. Dahn, *J. Electrochem. Soc.* **143,** 100 (1996).
4. M. M.Thackeray, M. F. Mansuetto, D. W. Dees, and D. R. Vissers, *Mater. Res. Bull.* **31,** 133 (1996).
5. M. M. Thackeray, M. F. Mansuetto, and C. S. Johnson, *J. Solid State Chem.* **125,** 274 (1996).
6. S. Bach, M. Henry, N. Baffier, and J. Livage, *J. Solid State Chem.* **88,** 325 (1990).
7. P. Barboux, J. M. Tarascon, and F. K. Shokoohi, *J. Solid State Chem.* **94,** 185 (1991).
8. W. Liu, G. C. Farrington, F. Chaput, and B. Dunn, *J. Electrochem. Soc.* **143** (3), 879 (1996).
9. W. Liu, K. Kowal, and G. C. Farrington, *J. Electrochem. Soc.* **143** (11), 3590 (1996).
10. Q. Zhang, A. Bonakdarpour, M. Zhang, Y. Gao, and J. R. Dahn, *J. Electrochem. Soc.* **144** (1), 205 (1997).
11. T. Takada, H. Hayakawa, and E. Akiba, *J. Solid State Chem.* **115,** 420 (1995).
12. T. Takada, H. Hayakawa, T. Kumagai, and E. Akiba, *J. Solid State Chem.* **121,** 79 (1996).
13. F. Izumi, *in* "The Rietveld Method" (R. A. Young, Ed.), pp. 236–253. Oxford Univ. Press, New York, 1993.
14. R. A. Young, *in* "The Rietveld Method" (R. A. Young, Ed.), pp. 1–38. Oxford Univ. Press, New York, 1993.
15. Japan Industrial Standard (JIS) M8233-1982, "Determination of Active Oxygen Content in Manganese Ores."
16. T. Takada, H. Hayakawa, E. Akiba, F. Izumi, and B. Chakoumakos, *J. Solid State Chem.* **130,** 74 (1997).
17. C. Masquelier, M. Tabuchi, K. Ado, R. Kanno, Y. Kobayashi, Y. Maki, O. Nakamura, and J. B. Goodenough, *J. Solid State Chem.* **123,** 255 (1996).
18. A. Yamada, *J. Solid State Chem.* **122,** 160 (1996).